Contemporary Engineering Sciences, Vol. 9, 2016, no. 8, 377 - 396
HIKARI Ltd, www.m-hikari.com
http://dx.doi.org/10.12988/ces.2016.614

Micro Indentation Hardness Testing of Commercial-Grade RDX Crystals

John F. Moxnes*, Øyvind Frøyland, Torbjørn Olsen, Tomas L. Jensen and Erik Unneberg

Land Systems Division, Norwegian Defence Research Establishment (FFI)
P.O. Box 25, NO-2027 Kjeller, Norway
*Corresponding author

Copyright © 2016 John F. Moxnes et al. This article is distributed under the Creative Commons Attribution License, which permits unrestricted use, distribution, and reproduction in any medium, provided the original work is properly cited.

Abstract

This paper describes the continuous micro indentation hardness testing of two commercial grades of RDX with differing shock sensitivities using three (3) different loads on a Berkovich indenter to obtain values of elastic modulus, hardness, and the fraction of elastic work. Indentation creep behavior was also investigated. All of this was performed in an effort to relate these mechanical property results to the materials' hot spot characteristics. While the two grades of RDX are known to have significantly different sensitivities, only minimal differences in the current hardness results were obtained.

Keywords: RDX, crystals, internal defects, micro indentation

1 Introduction

Quantitative methods have been developed to evaluate and characterize the quality of energetic particles to differentiate high quality energetic crystals from common used crystals. Most known is a pycnometer to measure particle density, scanning electron microscopy or optical microscopy to observe crystal morphology and internal defects, X-ray diffraction and nuclear quadrupole resonance to probe lattice effects. The shock sensitivity of RDX is influenced by many factors such as crystal size, crystal morphology, internal defects and surface defects. The internal defects at the micro range may be revealed by micro indentation measurements.

Sharma et al. (1997) examined the structure of crystal defects in damaged cyclotrimethylene trinitramine (RDX) ($C_3H_6N_6O_6$) during indentation, heat, or underwater shock using atomic force microscopy. It was concluded that RDX in its orthorhombic space group (Pbca), with a= 1.3182 nm, b= 1.1574 nm, c= 1.0709 nm, and z= 8 is a fragile solid. It loses integrity at stresses far below those required for any chemical reaction. Indentation generated a large number of triangular dislocation pits, which in their turn produced fissures, cracks and holes that merges. In the case of heating, in addition a large amount of delamination was shown. The thermal expansion coefficient differs in different direction of the crystal. During shock of 12.9 GPa the crystal becomes a three dimensional mosaic structure full of cracks and fissures with the size of 100- 500 nm. In all cases particles of the size 20-500 nm were ejected onto the surface as debris from the formation of defects.

In a reduced sensitivity RS-RDX round robin program optical microscopy was used with matching refractive index media for internal defects examination and contrasting refractive index media for morphology examination. The method had some ability to distinguish between different types of RDX (Watt et al. 2006). Results from internal defects showed that crystals type II RDX (RDX for short) had a higher number of small defects (less than 10 micron) compared to RS-RDX. The number of crystals that were cloudy/dark was less for RS-RDX. However, it was also shown that the number of crystals that were smooth was significantly higher for RS-RDX (Hudson et al. 2010). A large discrepancy in the total score of internal defects awarded by different labs was achieved (Watt et al. 2006). Hudson et al. (2011) concluded that Differential Scanning Calorimetry did not identify RS-RDX characteristics per se but was able to determine the presence of HMX in the RDX sample. Doherty and Watt (2008) found that although most RDX that exhibits low sensitivity had low HMX content, low HMX content was not sufficient to guarantee low sensitivity

Hagan and Chaudhri (1977) found Vickers hardness of 24.1 kg/mm^2 for single crystals of RDX of the size 10 mm x 5 mm x 2 mm grown in the laboratory when applying loads from 150-700 mN. RDX was obtained from recrystallization from solution in dimethylformaide. Cracks appeared with the Vickers diamond even for the smallest load. Assuming the Young's modulus of E=18.4 GPa, the fracture surface energy was 0.11 J/m^2 and 0.07 J/m^2 for two cleavage planes. It was assumed a Poisson ratio of 0.22 for the RDX. The surface energies compares with an estimate of 0.07 J/m^2 based on contact angle measurements (Elban 1979).

Halfpenny et al. (1984) measured Vickers hardness to 39 kg/mm^2 on slowly grown crystals of RDX in acetone. The crystals were prismatic and exhibited well developed faceting. It was concluded that the primary dislocation motion is in the (010) planes.

Chaudhri (1984) measured Vickers hardness to 24.1 MPa on laboratory grown RDX crystals in acetone.

Elban et al. (1984) report on Vickers micro hardness from 310-380 MPa on various growth faces of laboratory grown RDX crystals (50 gram load). For production grade Class D RDX the Vickers hardness was 290-490 MPa (100 gram load). Knoop hardness varies from 170 to 700 MPa for laboratory-grown RDX crystals (50 gram load) and varies from 210 to 770 MPa for production-grade Class D RDX.

Elban et al. (1989) and Elban et al. (1984) measured anisotropy by using Knoop hardness. Hardness was from 170-700 MPa.

Armstrong and Elban (1989) concluded based on Vickers micro indentation that RDX crystals are relatively easy to crack. The movement of dislocations is severely restricted and plastic flow at the residual indentation field is significantly localized. Vickers hardness measurement were made on a large as-grown surface of an un-mounted prismatic RDX crystal of apparent gem quality using a Tukon micro hardness tester for loads ranging between 25 and 250 g. A four point stage was used to level the crystal surface prior to each measurement. Hardness measurements were from 245-363 MPa, and the surface energy was 0.12 J/m^2. It was estimated that the minimum load for cracks to develop is 130 mN. The smaller the indentation size the greater the hardness.

Gallagher et al. (1992) showed orientation dependency of laboratory grown RDX crystals using micro hardness and the Knoop indenter. The variation of 32-44 kg/mm^2 was consistent with the crystallographic symmetry of the solids. The variation in hardness reflects the orientation of the dominant slip system.

Armstrong et al. (2002) show hardness comparison for elastic, plastic, and cracking behavior for a variety of energetic and inert crystals.

Ramos et al. (2009) report on nano indentation of a conical probe with 0.25-10 mN load on different faces of single crystals of RDX. The conical tip was used to investigate plasticity prior to cracking. All orientations show cracking behavior at very low loads. The maximum shear stress was within 1/15 to 1/10 of the shear moduli. Depending of the indentation surface the reduced elastic modulus was between 16.2 and 21.0 GPa. The indentation hardness (H_{it}) was also dependent of the indentation surface and hardness was between 615 and 672 MPa. Ramos et al. (2011) showed that smooth and habit planes of unprocessed single crystals of RDX exhibited distinct yield points near the theoretical shear strength while planes produced by cleavage yielded a lower applied stress.

Hudson et al. (2012) found by applying micro hardness tests at loads up to 200 mN and use of the Berkovich tip a difference in elastic modulus between commercial produced Chemring Nobel AS RS-RDX and RDX in their Table 3 and Table 4 (stiffness). The particles were grinded and polished. The reduced elasticity was from 16.6 to 18.0 GPa. The hardness was not reported but was calculated by using the reported stiffness to be 440-543 GPa (Weingarten and Sausa 2015).

Clayton and Becker (2012) developed an anisotropic constitutive model for single RDX crystals. Model predictions during spherical indentation for elastic response agreed with experimental data. It was suggested that surface and possible subsurface fractures that was not shown numerically may contribute to a loss of stiffness in experiments. The predicted Young's modulus varied from 15.40-20.85 GPa for indentation on different crystal planes. See also Antunes et al. (2006) and Sakarova (2009) for indentation simulations and Chen et al. (2008) for molecular nano-indentation simulation of energetic materials.

Weingarten and Sausa (2015) studied nano mechanics of RDX single crystals by force-displacement measurements using the Berkovich triangular indentation tip, and molecular dynamics simulations. The (210) surface exhibited more stiffness than the (001) surface. The (001) surface exhibits isotropic compression during indentation, whereas the (210) surface showed anisotropy during indentation at similar loads. The reduced modulus and the indentation hardness for the (210) surface were 22.9 GPa and 798 GPa respectively.

There are many similarities between the previous micro indentation results but the difference between suggested slip systems and material strength parameters in RDX have not been completely resolved. The differences may be attributed to the use of different crystallization techniques, loads, tip geometries, and grounding and polishing techniques. Numerical simulations of micro hardness may be useful tool for better understanding. Due to the morphological structure our commercial grade RDX needs to be embedded in an epoxy matrix and further grinded and polished to reveal a flat surface for hardness or elasticity measurements (Hudson et al. 2012, Bouma et al. 2013).

In this article we perform a somewhat limited, but practical number of indentation tests. We extract the Young's modulus (E_{it}), indentation hardness (H_{it}), creep (C_{it}), and fraction of elastic work (η_{it}), by using the Berkovich triangular indentation tip with loads up to 200 mN.

In Section 2 we show the set up. In Section 3 we present the results, whereas we conclude and make some discussions in Section 4.

2 The experimental set up and micro indentation analyses

A number of crystals/particles/grains of RDX and RS-RDX were delivered from Chemring Nobel AS. Standard RDX was not treated to obtain reduced sensitivity. Improved RDX was produced by Chemring Nobel AS to give a higher purity, good packing density, and a low viscosity in cast cure compositions. RS-RDX was based on improved RDX and was achieved by further post treatment to lower the sensitivity.

To obtain representative samples a number of RS-RDX crystals (10 mg) were arbitrary taken and placed into the mould. Resin was poured into the mould of height 1.5 cm and diameter 3.0 cm. The resin was allowed to cure for 24 hours at room temperature. After solidification, the surface containing embedded crystals was grounded for one minute using 1200 grit sandpaper and water to expose the crystals and provide a smooth surface. Further polishing for 0.5 minute with 0.05 μm alumina paste provided a mirror finish as seen in Figure 1. The same procedure was applied for RDX. All measurements were performed while using masks.

The micro indentation tests were performed on a Shimadzu Dynamic Ultra micro Hardness Tester (DUH-211S). A Berkovich indenter (Triangular 115°) was employed, and the tip area was calibrated using a reference specimen of fused quartz. Analysis of the tip calibration and the calculation of the elastic modulus, hardness, and creep followed the Oliver Pharr method (ISO14577-1).

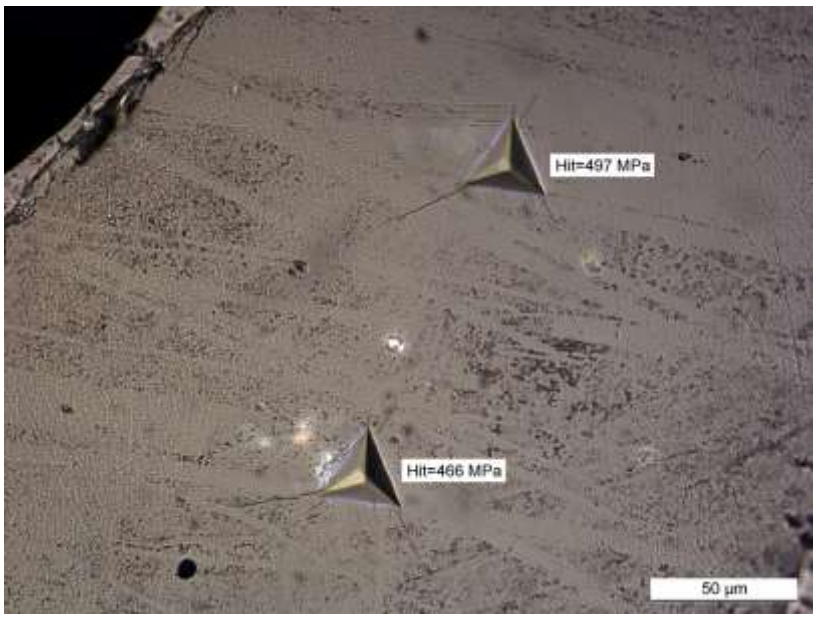

Figure 1: Two indentations in RDX at maximum force of 200 mN RS-RDX, 20141021. The surface is grinded and polished

We construct an indentation matrix with a number of indents in each crystal. The load control method is used. The maximum forces were 10 mN, 100 mN or 200 mN. The loading rates were 0.4777 mN/s, 4.4413 mN/s, and 10.0096 mN/s respectively. The holding times at maximum force were 5 seconds as baseline, but for some of the tests we use 30 second (see Figure 5).

For each measurement force vs time (Figure 2) and depth vs time (Figure 3) were produced as two data sets. From these two data sets Young's modulus, hardness, creep, and fraction of elastic work were calculated.

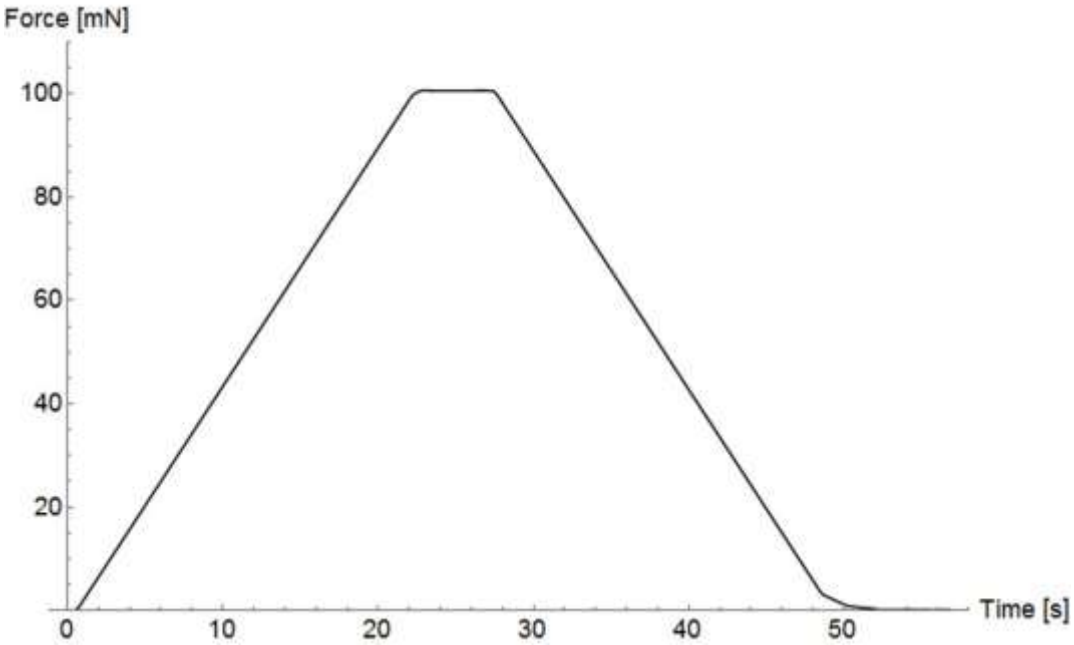

Figure 2: The Force (load) in mN versus time in seconds during indentation. RS-RDX, 20141015, 100mN

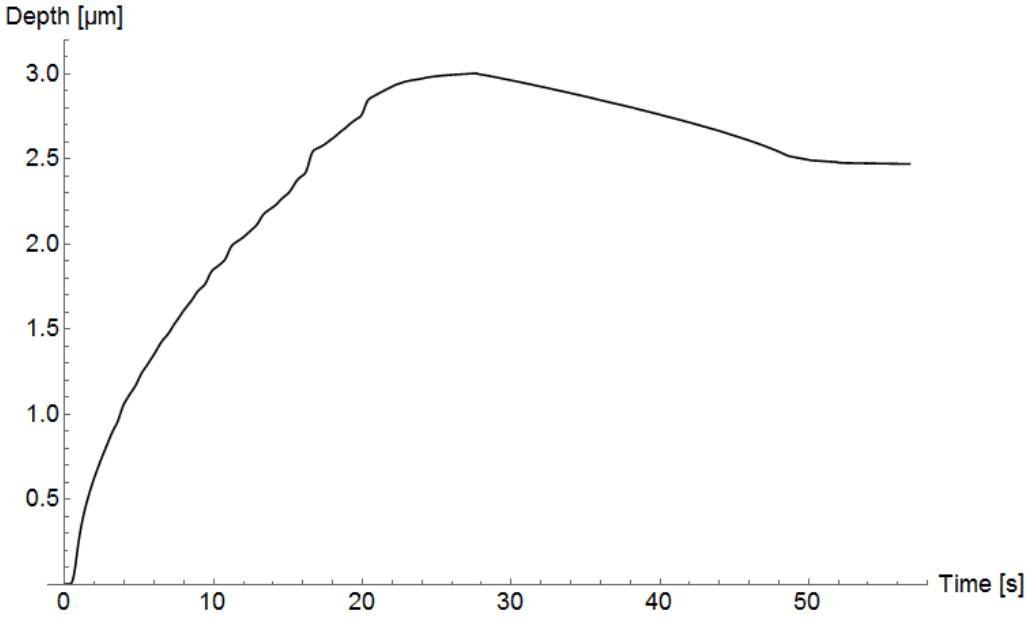

Figure 3: The depth in µm versus time in seconds during indentation. RS-RDX, 20141015, 100mN

The specimen Young's modulus $E_s = E_{it}$ is calculated by

$$\frac{1-\nu_s^2}{E_s} = \frac{1}{E_r} - \frac{1-\nu_i^2}{E_i},\ E_s = E_{it} \tag{2.1}$$

where E and ν are the Young's modulus and the Poisson's ratio, respectively, of the specimen (s) and of the indenter (i). We set that E_i = 1.14 10^{12} Pa, and ν_i = 0.07 for the diamond tip (Weingarten and Sausa 2015). The Poisson ratio for the specimen is set to ν_s = 0.22 (Hudson et al. 2012). Equation (2.1) needs the reduced elasticity E_r which is calculated as

$$E_r = \frac{\sqrt{\pi}}{2\beta}\frac{1}{\sqrt{A_p}}\frac{1}{C} \tag{2.2}$$

where A_p is the projected contact area at maximum force (immediately before unloading) and $C = dh/dF$ is the compliance, where *S= 1/C* is called the stiffness. We set that β = 1.034 for the Berkovich (Triangular 115°) indenter.

Further for the triangular indenter we calculate the projected area at maximum load according to the traditional formulae

$$A_p = 23.96 \times \left(h_{max} - \varepsilon\left(h_{max} - h_r\right)\right)^2, \ \varepsilon = 3/4 \tag{2.3}$$

where h_r is the projected depth after unloading (The crossing between the force vs. depth-axis and the tangential line of the reloading curve drawn at maximum load. See Figure 4). The H_{it} hardness is calculated as

$$H_{it} = \frac{F_{max}}{A_p} \tag{2.4}$$

The creep C_{it} and the fraction of the elastics work η_{it} are calculated as (Figure 4)

$$C_{it} = \frac{h_{max} - h_1}{h_1} \times 100, \ \eta_{it} = \frac{W_e}{W_e + W_p} \times 100 \tag{2.5}$$

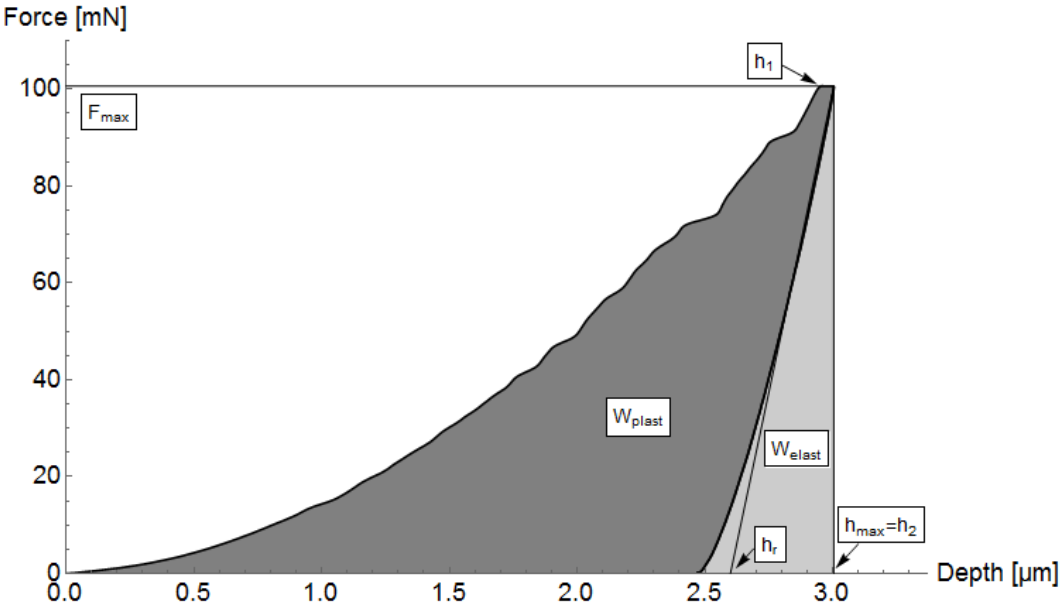

Figure 4: The force (load) vs depth with important parameters defined. RS-RDX, 20141015, 100mN

3 Results

Figure 5 shows all our results for the Young's modulus (E_{it}). We use maximum force (load) of 10 mN, 100 mN, and 200 mN. Each column corresponds to one measurement, and each group of columns corresponds to one, two, or five crystals. The number of crystals in use is denoted in the Figures.

Figure 6 and 7 show the average and median. To check the significance between groups we use the standard deviation when applying average, and the mad (mean average difference) when applying median. The mad is calculated by taking the median of the difference between the median and the data. The median and the mad increase robustness for outliers in the conclusions (Amc Technical brief 2001).

For the 10 mN force in Figure 6 the difference between RDX and RS-RDX is insignificant both when using average together with standard deviation, and when using median together with mad. The same conclusion applies for the 100 mN and the 200 mN force. It can be seen that E_{it} decreases with increasing load. This is in agreement with Hudson et al. (2012) and Weingarten and Sausa (2015). Probably, increasing loads decreases crystal strength and hardness due to cracking. The elastic modulus is measured during unloading and thus after maximum force. If maximum force is above the strength of the crystal cracks are developed. It is reason to believe that the elastic modulus is influenced by the number cracks in the crystal that may increase with the load (see also Figure 3 in Hudson et al. 2012 and Figure 5 in Weingarten and Sausa 2015). It can be speculated that the 200 mN RDX has larger E_{it} than 200 mN RS-RDX, but the difference is not significant. The 100 mN with the holding time of 30 seconds is not significantly different from the 100 mN with the baseline holding time (5 seconds).

Figure 7 shows the calculated hardness H_{it} for all the tests, while Figure 8 shows the statistics. The hardness decreases with load, and no significant difference between RS-RDX and RDX are seen. The holding time does not influence the hardness.

Figure 9 and 10 show the creep C_{it}. The scatter is large. The RS-RDX and the RDX show no significant difference. The creep did not depend significantly on the load, and the dependency of holding time is insignificant.

Figure 11 and 12 show the fraction η_{it} of the elastic work. The RS-RDX 100 mN shows lower fraction of elastic work than the 10 mN and 200 mN. However, the RS-RDX 100 mN results are based on only one crystal. We see that the 100 mN that use of five crystals (and 30 s holding time) is not significantly different from the 10 mN or the 200 mN. It seems that the test with one grain of 100 mN RS-RDX has lower fraction of elastic work. It is suggested that fraction of elastic work

differs more between crystals than within crystals. 200 mN RS-RDX shows significantly higher η_{it} than other cases. However, this conclusion is based on the use of median and the mad alone.

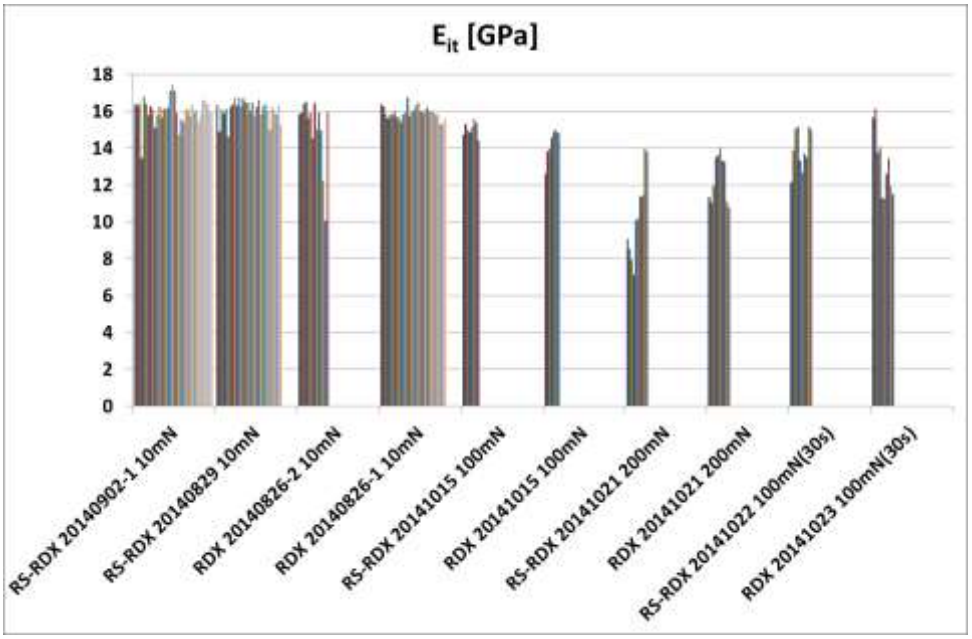

Figure 5: The elasticity modulus for the various tests. Each group is one, two or five crystal surfaces and each column is one indent

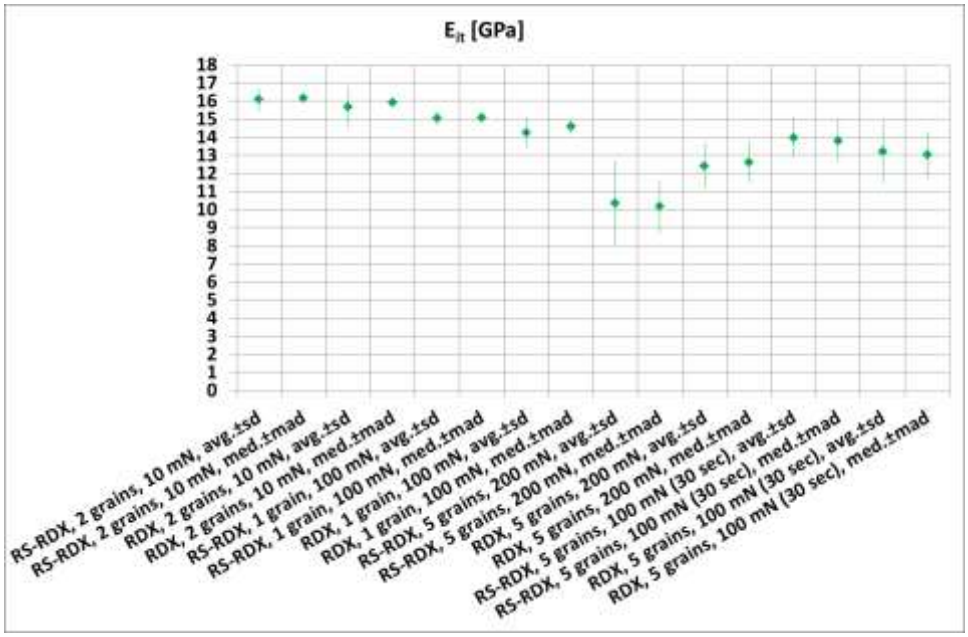

Figure 6: The statistics of the elasticity modulus for the various tests

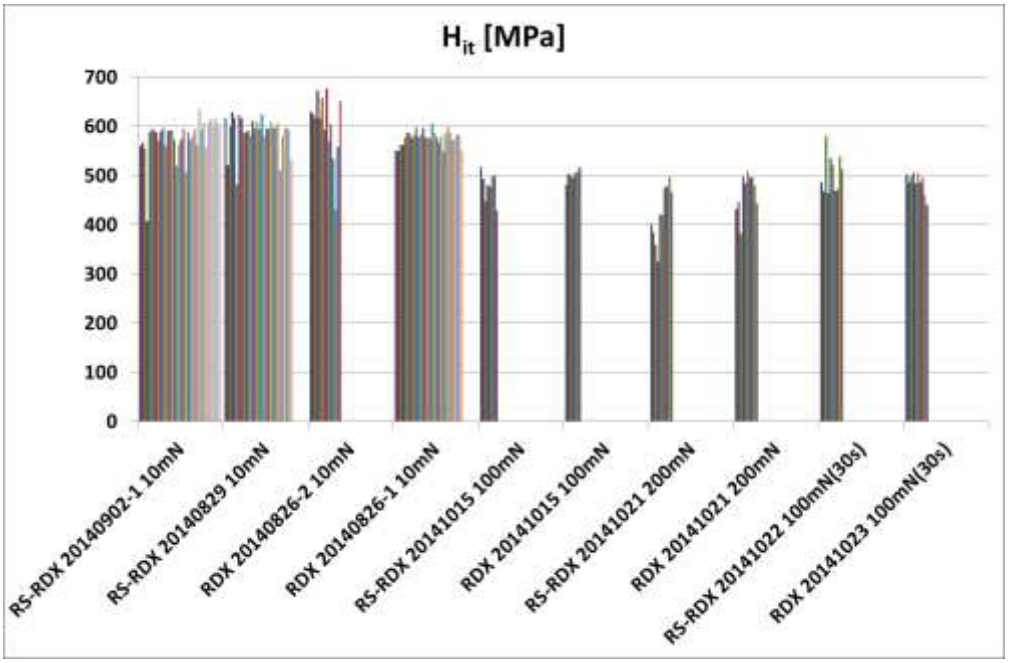

Figure 7: The hardness for the various tests

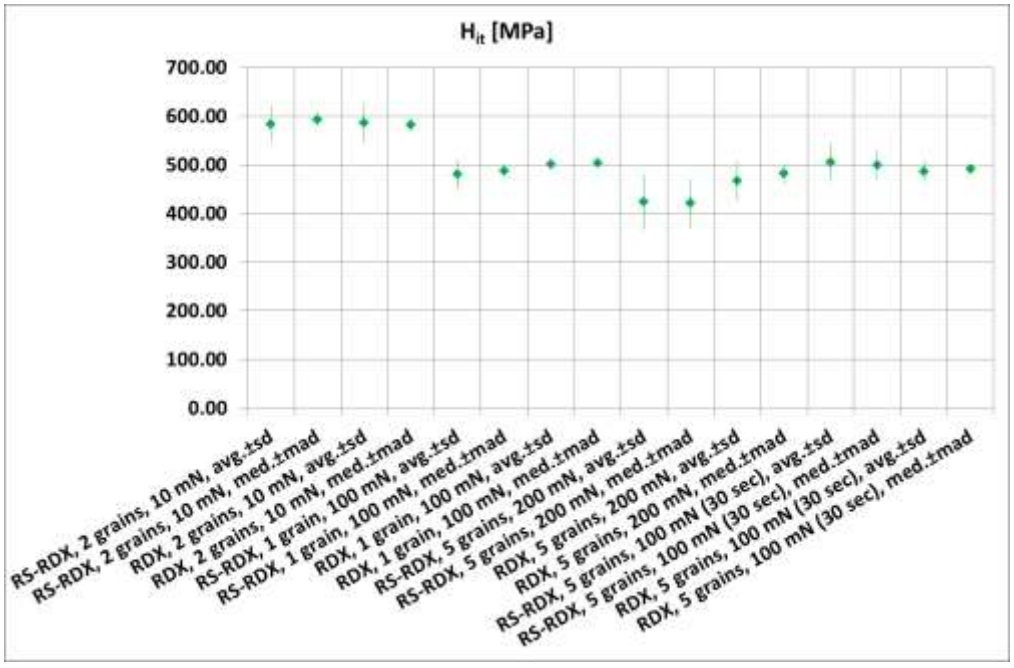

Figure 8: The statistics of the hardness for the various tests

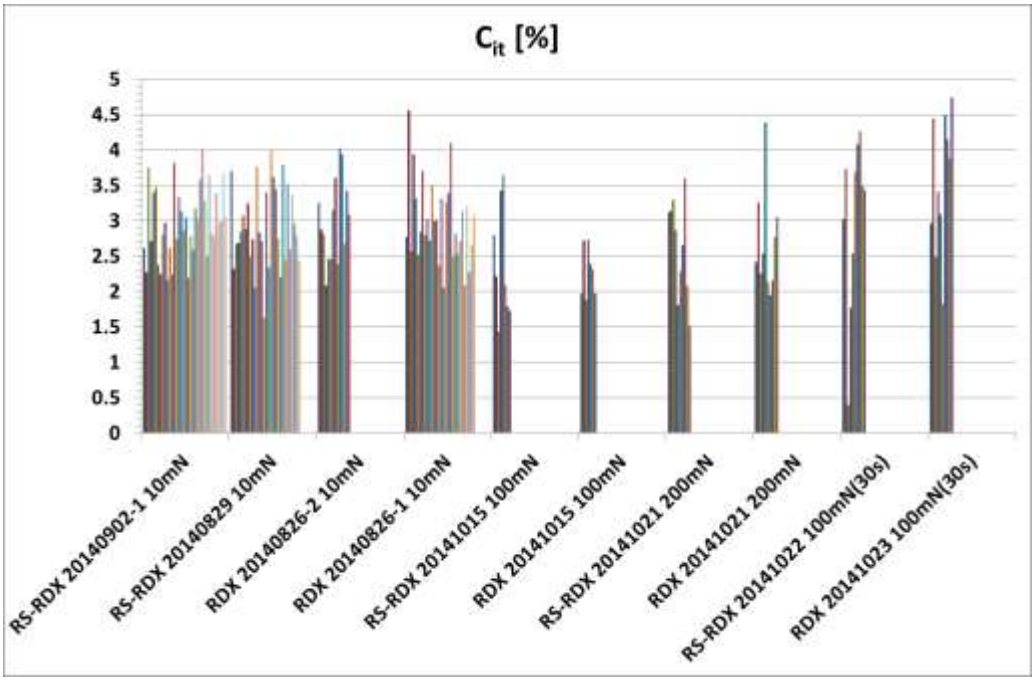

Figure 9: The creep for the various tests

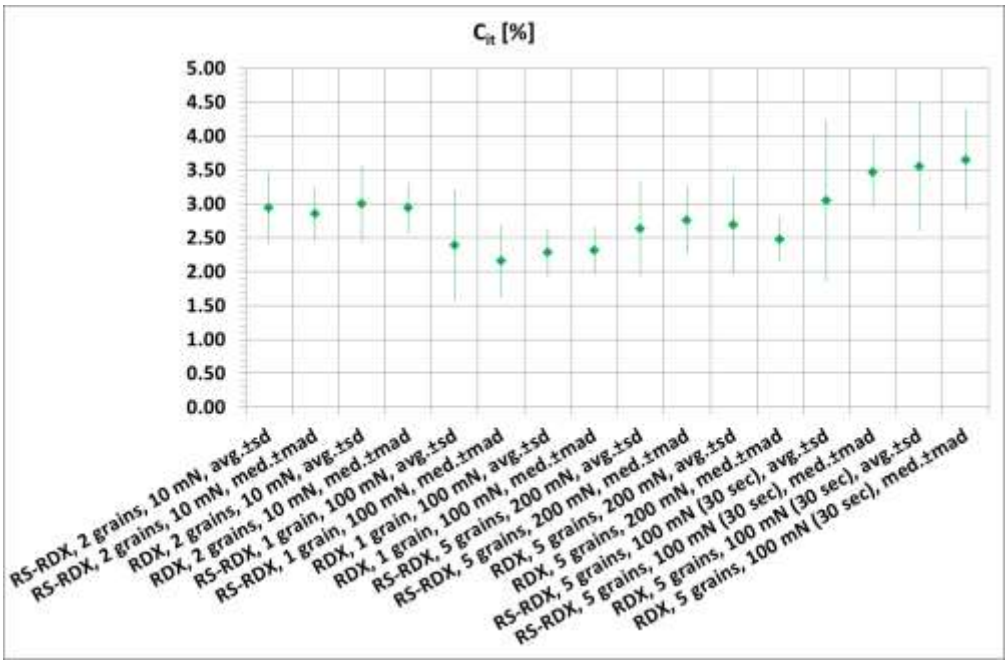

Figure 10: The statistics of the creep for the various tests

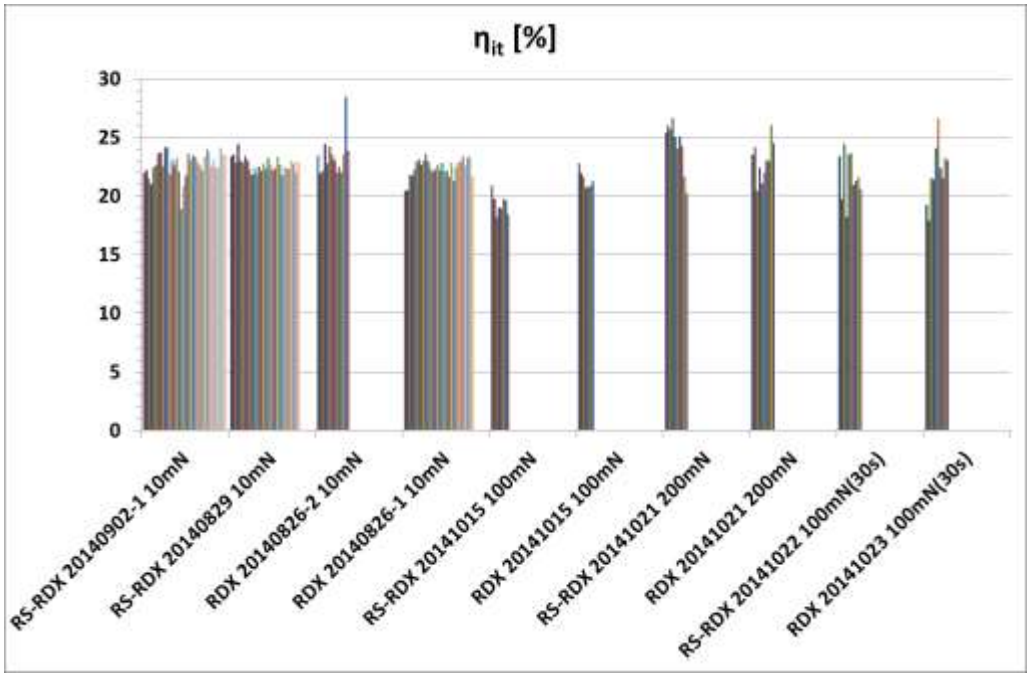

Figure 11: The fraction of the elastic work for the various tests. Each group is one particle surface and each column is one indent

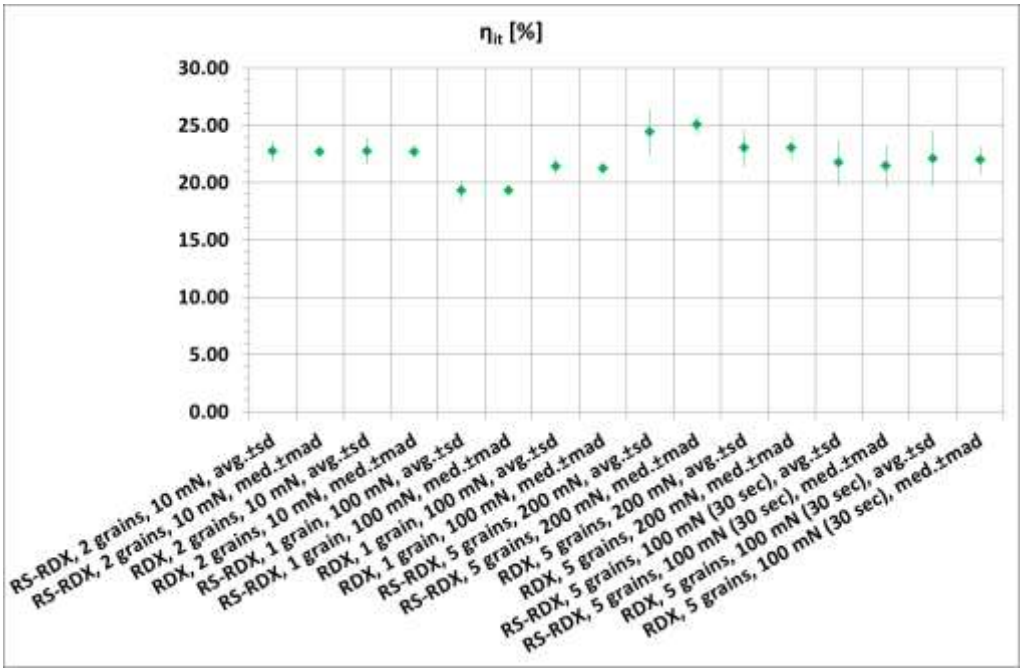

Figure 12: The statistics of the fraction of elastic work for the various tests

Hudson et al. (2012) find for RDX Young's modulus of around 16 GPa, 14.5 GPa and 13.5 GPa for the loads 10 mN, 100 mN and 200 mN loads respectively. These values for RDX agree with our results in Figure 6. However, the Young's modulus of RS-RDX of Hudson et al. (2012) is significant higher than our values. Hudson et al. (2012) report on fraction of elastic work at 200 mN in their Figure 6 and Figure 8. Their elastic work did not show any correlation to defects of crystals (Figure 6 in their paper). RS-RDX shows fraction of elastic work around 20 % while RDX shows values around 21 %. These values are lower than presented in this article (Figure 12). In Figure 13 and Figure 14 we sum up different results in the literature. Both the E_{it} and H_{it} are decreasing with the load. In Figure 15 we have used the stiffness values of Hudson et al. (2012) to calculate indentation hardness. Hardness decreases with increasing load. The exception is the 200 mN for RDX (Figure 15). It is notable that the nano indentation of Ramos et al. (2009, 2011) with the smallest load shows high E_{it} and high H_{it}. This underscores that both elasticity modulus and hardness decreases with the load. Thus cracks are likely developed during indentation. The elastic modulus is probably influenced by the number cracks in the crystal that may increase with the load (see also Figure 3 in Hudson et al. 2012 and Figure 5 in Weingarten and Sausa 2015).

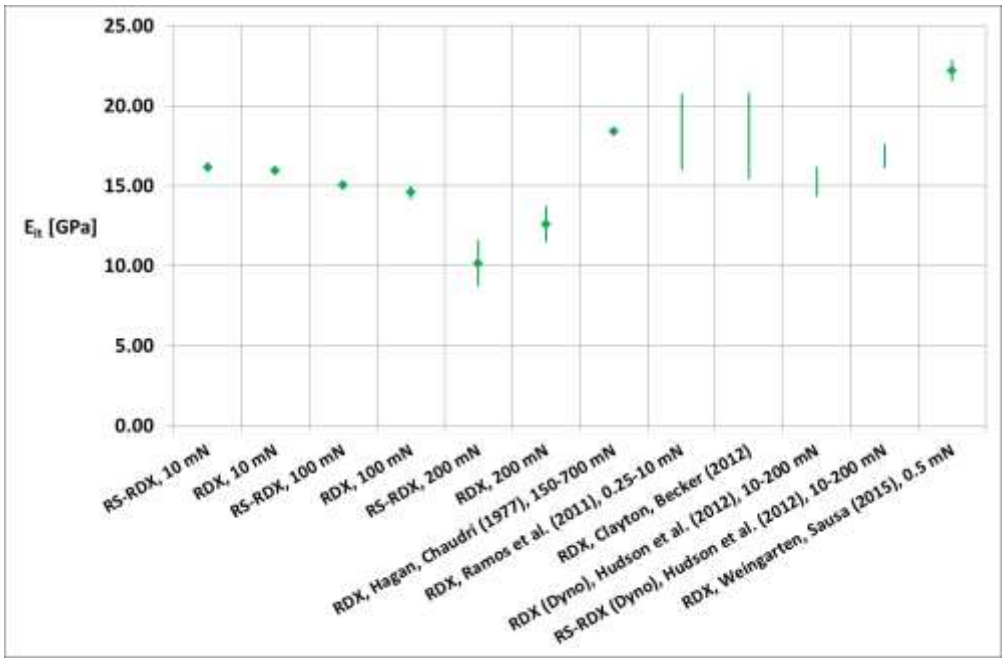

Figure 13: The statistics of the elastic modulus for the various tests in the literature. Note that the range of the literature values are based on reported min and max values. Error bars of Weingarten and Sausa (2015) are based on standard deviation

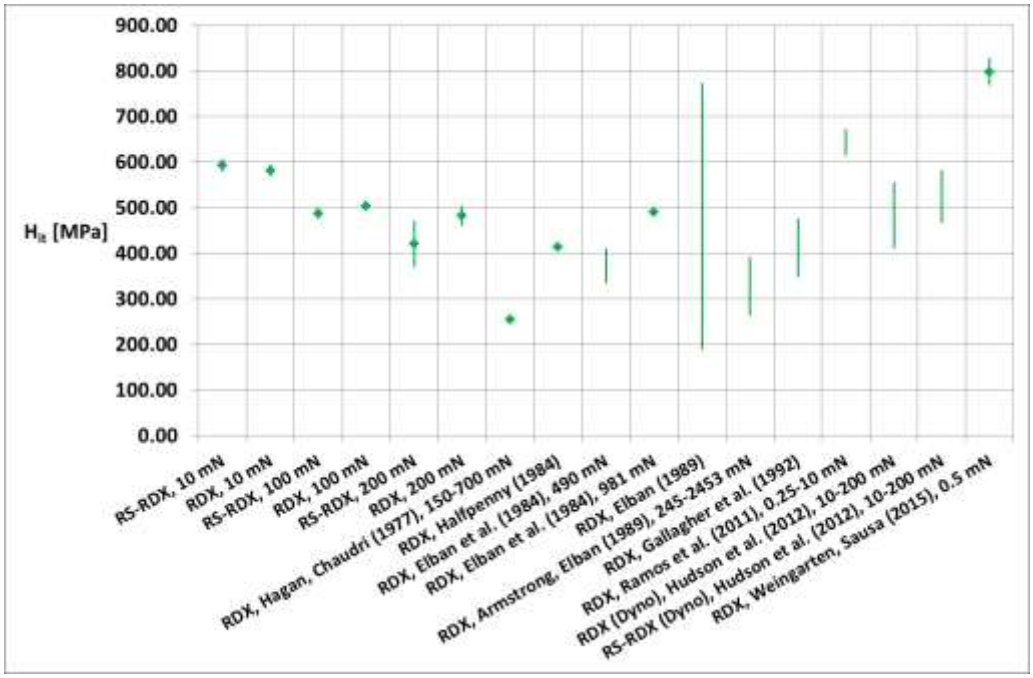

Figure 14: The statistics of the hardness for the various tests in the literature. Note that the range of the literature values are based on reported min and max values. Error bars of Weingarten and Sausa (2015) are based on standard deviation

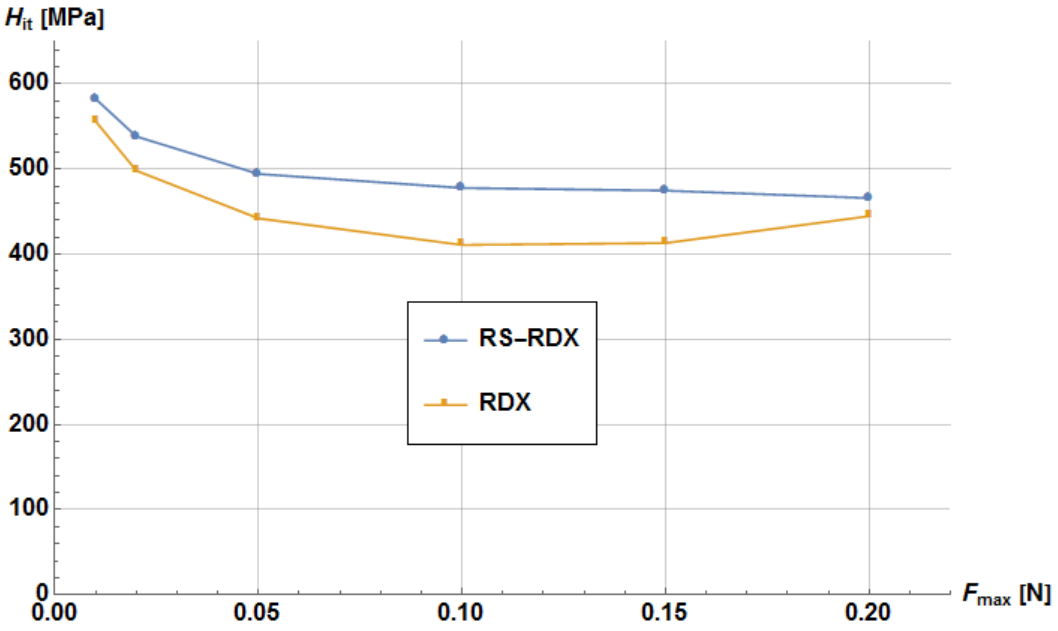

Figure 15: The hardness based on Hudson et al. (2012) stiffness data

Summarizing: The Young's modulus and indentation hardness decrease with increasing load. Measurement of creep was not useful for any conclusions. The scatter in the data simply seems too large. Fraction of elastic work shows some interesting result. It appears that the elastic fraction is significant lower at 100 mN than at 10 mN and 200 mN for one particular crystal. It may be that for the fraction of elastic work, differences between crystals are larger than differences within crystals. The 200 mN RS-RDX shows larger elastic fraction than other cases. However, the conclusion is based on the median together with the mad, and it does not follow when using average together with standard deviation.

4 Summary and conclusions

We measured the elasticity, hardness, creep, and fraction of elastic work of two different types of RDX. The effect of holding time at max force was also studied. The reduced sensitivity Chemring Nobel AS RDX is known to be less sensitive than traditional RDX in shock test but we did not find significant differences between RDX and the reduced sensitivity RDX in Young's modulus or indentation hardness. The Young's modulus and the hardness decreased with increasing load from 10 mN to 200 mN. The scatter in creep was too large to be useful for any conclusions. Holding time at maximum force did not influence the results. The 200 mN RS-RDX shows larger elastic fraction than other cases.

Hudson et al. (2012) found by applying micro hardness tests differences in elastic modulus between Chemring Nobel AS RS-RDX and RDX in their Table 3 and Table 4. A difference may not be statistically significant unless a large and almost impractical number of tests are performed. In addition a question is how to cope with often observed outliers in the statistical material. It is notable in this regard that it may be that the number of tests we performed in this article were not many enough to reveal significant differences in elasticity and indentation hardness between RDX and RS-RDX. However, our data clearly revealed that Young's modulus and hardness decrease with increasing load. This may be seen as a validation of the results. Increasing loads on crystals decreases strength and hardness due to cracking. We may forecast that differences in fraction of elastic work between crystals are larger than differences within crystals.

The necessary use of a very large number of tests to reveal difference between RS-RDX and RDX may lead to impracticality of the hardness test for our application. Further studies are necessary to reveal this matter and to examine whether RDX compared to RS-RDX may show a small number of crystals with a high number of internal defects that acts as triggers for reaction during shock.

Acknowledgement. We thank Ph.D. Tor Erik Kristensen at FFI for interesting discussions during the preparation of this manuscript.

References

[1] J.M. Antunes, L.F. Menezes, J.V. Fernandes, Three-dimensional numerical simulation of Vickers indentation tests, *Int. J. Solids Structures*, **43** (2006), 784-806. http://dx.doi.org/10.1016/j.ijsolstr.2005.02.048

[2] Amc Technical brief, Analytical Methods Committee, (2001), nr 6.

[3] R.W. Armstrong, W.L. Elban, Cracking at hardness nicro-indentations in RDX explosive and MgO single crystals, *Matr. Sci. Eng. A*, **111** (1989), 35-43. http://dx.doi.org/10.1016/0921-5093(89)90195-0

[4] R.W. Armstrong, H.L. Ammon, W.L. Elban, D.H. Tsai, Investigation of hot spot characteristics in energetic crystals, *Thermochimica Acta*, **384** (2002), 303-313. http://dx.doi.org/10.1016/s0040-6031(01)00786-9

[5] R.H.B. Bouma, W. Duvalois, A.E.D.M. Van der Heijden, Microscopic characterization of defect structure in RDX crystals, *J. Microscopy*, **252** (2013), no. 3, 263-274. http://dx.doi.org/10.1111/jmi.12088

[6] M.M. Chaudhri, The deformation stress of highly brittle explosive crystals from real contact area measurements, *J. Materials Science*, **19** (1984), 3028-3042. http://dx.doi.org/10.1007/bf01026982

[7] J.D. Clayton, R. Becker, Elastic-plastic behavior of cyclotrimethylene trinitramine single crystals under spherical indentation: Modelling and simulation, *J. Appl. Phys*., **111** (2012), 111-120. http://dx.doi.org/10.1063/1.3695392

[8] Y.C. Chen, K.I. Nomura, R.K. Kaila, A. Nakano, P. Vashishta, Molecular dynamics nanoindentation simulation of an energetic material, *Appl. Physics Letters*, **93** (2008), 93-94. http://dx.doi.org/10.1063/1.3006428

[9] R.M. Doherty, D.S. Watt, Relationship between RDX properties and sensitivity, *Prop. Exp. Pyrotechnics*, **33** (2008), no. 1, 4-13. http://dx.doi.org/10.1002/prep.200800201

[10] W.L. Elban, Surface energies of high explosives PETN and RDX from contact angle measurements, *J. Mat. Sci. Lett.*, **14** (1979), 1008-1011.

[11] W.L. Elban, J.C. Hoffsommer, R.W. Armstrong, X-ray orientation and hardness experiments on RDX explosive crystals, *J. Materials Science*, **19** (1984), 552-566. http://dx.doi.org/10.1007/bf02403243

[12] J.T. Hagan, M.M. Chaudhri, Fracture surface Energies of high explosives PETN and RDX, *J. Mater. Sci.*, **12** (1977), 1055-1058. http://dx.doi.org/10.1007/bf00540993

[13] H.G. Gallagher, P.J. Halfpenny, J.C. Miller, J. N. Sherwood, D. Tabor, Dislocation slip systems in pentaerythritol tetranitrate (PETN) and cyclotrimethylene trinitramine (RDX) [and Discussion], *Phil. Trans. R. Soc. A*, **339** (1992), 293-303. http://dx.doi.org/10.1098/rsta.1992.0036

[14] P.J. Halfpenny, K.J. Roberts, J.N. Sherwood, Dislocations in energetic materials, *J. Materials Science*, **19** (1984), 1629-1637. http://dx.doi.org/10.1007/bf00563061

[15] R. Hudson, P.P. Gill, P.Q., Flower, A.S. Cumming, Assessment of RDX crystal morphology and defects, Study of RS-Nitramines (UKE/WPE/Taks005/007), (2010).

[16] R. Hudson, P.P. Gill, P.Q. Flower, A.S. Cumming, Thermal analysis of RDX using Differential Scanning Calorimetry, Working paper, (2010).

[17] R.J. Hudson, P. Zioupos, P. Gill, Investigating the mechanical properties of RDX crystals using nano-indentation, *Propellants Explos. Pyrotech.*, **37** (2012), 191-197. http://dx.doi.org/10.1002/prep.201100063

[18] L. Ming, H. Ming, K. Bin, W. Maoping, L. Hongzhen, X. Rong, Quality evaluation of RDX crystalline particles by confined quasi-static compression method, *Prop. Exp. Pyrot.*, **32** (2007), no. 5, 401-405. http://dx.doi.org/10.1002/prep.200700043

[19] K.J. Ramos, D.E. Hooks, D.F. Bahr, Direct observation of plasticity and quantitative hardness measurements in single crystal cyclotrimethylene trinitramine by nanoindentation, *Philosophical Magazine*, **89** (2009), no 27, 2381-2402. http://dx.doi.org/10.1080/14786430903120335

[20] K.J. Ramos, D.F. Bahr, D.E. Hooks, Defect and surface asperity dependent yield during contact loading of an organic molecular single crystal, *Philosophical Magazine*, **91** (2011), no. 7-9, 1276-1285. http://dx.doi.org/10.1080/14786431003745336

[21] N.A. Sakharova, J.V. Fernandes, J.M. Antunes, M.C. Oliveira, Comparison between Berkovich, Vickers and conical indentation tests: A three-dimensional numerical simulation study, *Int. J. Solids and Structures*, **46** (2009), 1095-1104. http://dx.doi.org/10.1016/j.ijsolstr.2008.10.032

[22] J. Sharma, S.M. Hoover, C.S. Coffey, A.S. Tompa, H.W. Sandusky, R.W. Armstrong, W.L. Elban, Structure of crystal defects in damaged RDX as revealed by AFM, CP429, Shock Compression of Condensed Matter ed. Schmidt/Dandekar/Forbes, (1997), 563-566.

[23] D.S. Watt, R.M. Doherty, L. Nock, RS-RDX Round Robin (R4) preliminary Results Analysis, MSAIC, Report L-127, (2006).

[24] N.S. Weingarten, R.C. Sausa, Nanomechanics of RDX single crystals by force-displacement measurements and molecular dynamics simulations, *The J. Physical Chemistry A*, **119** (2015), 9338-9351. http://dx.doi.org/10.1021/acs.jpca.5b04876

Appendix

The Vickers hardness, Berkovich hardness, and the Knoop hardness are defined by the force divided by the contact area (true contact area) after unloading the force. However, the indentation hardness which we use in this article is (for any tip geometry) the force divided with the projected area at maximum force.

The relationship between the projected A_p and the true contact area A_s varies between the geometrical forms of the indenters. The projected area (square) of the Vickers hardness is $A_p = d^2/2$, where d is the length of the diagonal in the square. Geometrical considerations gives that $A_s = A_p / \ Sin(136°/2) = d^2/(2\ Sin(136°/2)) = d^2/1.8544$. Thus

$$HV = \frac{F}{A_s} = \frac{F}{d^2} 2\,Sin(136°/2), F = \frac{9.81 \times VHN}{1.8544} d^2 \quad \text{(A1)}$$

Here *VHN* is the Vickers hardness in kg/mm^2. The projected area of the Berkovich tip is $A_p = l^2\sqrt{3}/4$, where l is the length of the sides of the projected triangle. The contact area is

$$A_s = \frac{2A_p}{Tan\left(115.12°/2\right)} = l^2 \frac{\sqrt{3}}{2Tan\left(115.12°/2\right)} \tag{A2}$$

In the Knoop hardness test geometry of this indenter is an extended pyramid with the length to width ratio being 7:1 and respective face angles are 172° for the long edge and 130° for the short edge. It can be shown that

$$A_s = 1.10559A_p \tag{A3}$$

Received: January 26, 2016; Published: April 21, 2016